Potential Energy Curves and Geometrical Structure Variations for ($[MX_4]^{2-}$: M=Ni(II), Pd(II), Pt(II); X=Cl^-, Br^-) Dissociating into ($[MX_3]^- + X^-$) : *Ab Initio* Study

Jong Keun Park,* Bong Gon Kim, and In Sun Koo

*Department of Chemistry Education and Research Institute of Basic Science, Gyeongsang National University, Jinju 660-701, Korea. *E-mail: mc7@gsnu.ac.kr*

Received April 13, 2005

Potential energy curves and internuclear (M-X) distance variations for dissociation reactions of $[MX_4]^{2-}$ into ($[MX_3]^- + X^-$) have been calculated using *ab initio* Hartree-Fock (HF), second order Möller-Plesset perturbation (MP2), and Density Functional Theory (DFT) methods with a triple zeta plus polarization (TZP) basis set. The equilibrium geometrical structures of $[MX_4]^{2-}$ are optimized to tetrahedral geometry for $[NiX_4]^{2-}$ and square planar geometry for ($[PdX_4]^{2-}$ and $[PtX_4]^{2-}$). The bond (M-X) distances of $[NiCl_4]^{2-}$, $[NiBr_4]^{2-}$, $[PdCl_4]^{2-}$, $[PdBr_4]^{2-}$, $[PtCl_4]^{2-}$, and $[PtBr_4]^{2-}$ at the DFT level are 2.258, 2.332, 2.351, 2.476, 2.367, and 2.493 Å, respectively. The dissociation energies for the bond dissociation of ($[MX_3]^- \cdots X^-$) at the DFT level are found to be 4.73 eV for $[NiCl_4]^{2-}$, 4.89 eV for $[NiBr_4]^{2-}$, 4.93 eV for $[PdCl_4]^{2-}$, 5.57 eV for $[PdBr_4]^{2-}$, 5.44 eV for $[PtCl_4]^{2-}$, and 5.87 eV for $[PtBr_4]^{2-}$. As the (M$\cdots$X) distance of ($[MX_3]^- \cdots X^-$) increases, the distance variation (**R**t) of *trans* (M-X) bond at the *trans*-position is shorter than those (**R**c) of two *cis* (M-X) bonds at the *cis*-position. Simultaneously the atomic charge variation of *trans*-X atom is more positive than those of equilibrium $[MX_4]^{2-}$ structures, while the variation of leaving X group is more positive.

Key Words : Potential energy curve, Geometrical structure, Dissociation reaction, Atomic charge, Density functional theory

Introduction

The geometrical structures,[1-11] ligand exchange reactions,[12-20] and catalytic reactions[21-23] of nickel, palladium, and platinum complexes ($[MX_4]^{2-}$) have been one of the issues of various theoretical and experimental approaches. In particular, many of these have focused on the catalytic properties[21-23] for nickel and palladium complexes and on the antitumorous properties[12-20] for platinum complexes. The electronic[1-5] and geometrical[6-20] structures of these complexes have been investigated and compared theoretically. And the other properties were also explored with numerous experimental works.[24-46] These geometrical structures of $[MX_4]^{2-}$ are similar to each other, while the electronic structures are different. That is, the ground electronic configuration of the palladium complexes is $4d^{10}$ with a closed d-shell as a ^1S state, while the configuration of the platinum complexes is $5d^9 6s^1$ as a ^3D state. In previous some studies, the differences of the properties between these complexes were explained with the electronic configurations of Pd(II) and Pt(II) complexes.

The reaction mechanisms for the ligand exchange of the Ni(II), Pd(II), and Pt(II) complexes have been studying.[12-23] The ligand exchange at a metal center is proceeded *via* a trigonal bipyramidal geometry (D_{3h}) of the five coordinate transition state ($[PdL_5]^‡$) or *via* a C_{2v}-transition state symmetry. In the studies of Deeth group,[12-14] the ligand exchange reactions was theoretically suggested to be occurred *via* a vertically associative mechanism leading C_{2v}-transition state symmetry ($[PdL_5]^‡$). In the transition state, the structure of $[PdL_5]^‡$ is not rigorous trigonal bipyramidal geometry (D_{3h}). The C_{2v}-transition state structure of $[PdL_5]^‡$ is very similar to trigonal bipyramidal structure both energetically and geometrically. In their ligand exchange studies, the structure of $[PdL_5]^‡$ with D_{3h} symmetry is not the true transition state of an associatively activated mechanism. The energetic diagrams of the hydration processes for palladium and platinum complexes were examined by Burda *et al.*[15-17,20] With various computational methods, the replacement of ligands (NH_3, H_2O, OH^-) from $[Pd(NH_3)]^{2+}$ to $PdCl_4^{2-}$ shows a slightly endothermic or exothermic process by about 100 kcal/mol. In water solution state, two vertical metal-oxygen interactions of the apical positions in the square planar $PdCl_4^{2-}$ and $PtCl_4^{2-}$ complexes were experimentally observed by Caminiti *et al.*[35-36] The interaction between the complex and the solvent in aqueous solutions was suggested to be originated from the solubility of $PdCl_4^{2-}$ and $PtCl_4^{2-}$ complexes. With replacement of one or more Cl^- ions with water molecules, the possible solvation mechanisms of the ligand exchange in the square-planar complexes implies ligand-solvent interaction and/or metal-solvent interaction. The M-Cl distance of square-planar $[MCl_4]^{2-}$ units was found to be 2.315 Å, while the M-O distance of the metal-H_2O interactions bonded to the apical position is 2.77 Å.

In catalytic reactions, the formation of the stable (K[(alkene)MCl_3]) complexes and the coordination of ethene to the MCl_3^- species are estimated by the quantum chemical calculations.[21-23] The metal-olefin complexes are formed by the interaction between the anion of $[PtCl_3]^-$ and orbital of C_2H_4. On the basis of the EHT calculation, the magnitude of the change of the C=C torsional barrier in

Zeise anion alkenic complexes and the catalytic activities of Pd(II) and Pt(II) complexes were investigated by Ponec and Řeřicha.[23] The dissociation energies of the M-Cl bonds of $[PdCl_4]^{2-}$ and $[PtCl_4]^{2-}$ are only obtained from the potential energy differences between $[PdCl_4]^{2-}$ and ($[PdCl_3]^- + Cl^-$) and between $[PtCl_4]^{2-}$ and ($[PtCl_3]^- + Cl^-$), respectively. The geometrical structures of $M(PH_3)XY$, the relative energies of the *trans* and *cis* isomers, and the binding energies of the metal-olefin complexes of $[M(Cl_3)(C_2H_4)]^-$ are obtained by Noell and Hay.[21,22]

Although the geometrical structures, energetics, and population analysis of the ($ML_2 + XY \leftrightarrow ML_2XY$) formation and dissociation processes by the ligand exchange reactions have been investigated theoretically and experimentally, further investigations of the reaction mechanisms through the exchange processes have not been cleared so far. In the present work, we have studied the potential energy curves for the dissociation of $[MX_4]^{2-}$ into ($[MX_3]^- + X^-$). Firstly, the equilibrium geometrical structures of $[MX_4]^{2-}$ were optimized at the MP2 and DFT levels. Secondly, the geometrical structures at each internuclear distance were optimized to obtain the geometrical parameters and atomic charges of $[MX_4]^{2-}$ dissociating into ($[MX_3]^- + X^-$). Lastly, the potential energy curves and the bond length variations were represented along the (M-X) bond dissociation coordinate.

Computational Methods

The equilibrium geometrical structures of ($[MX_4]^{2-}$: M=Ni(II), Pd(II), Pt(II); X=Cl^-, Br^-) were fully optimized with the Hartree-Fock (HF), second-order Möller-Plesset (MP2), and density functional theory (DFT) levels using the Gaussian 03.[47] In addition, the geometrical structures of the ground states of $[MX_4]^{2-}$ were also optimized with the singly and doubly excited configuration interaction (SDCI) method using the GAMESS package. To confirm the existence of the stable structures, the harmonic vibrational frequencies of the species have been analyzed at the Hartree-Fock and density functional theory levels.

The basis sets chosen are the double zeta basis on Ni (3s3p3d/3s2p2d),[48,49] Pd (3s3p4d/3s2p2d),[21,22] and Pt(4s4p5d/3s3p2d).[21,22] The polarization functions[15-17] were used for Ni(II) (s-, p-, and d-functions: α_s = 0.009, α_p = 0.011, α_d = 0.04), Pd(II) (α_s = 0.008, α_p = 0.012, α_d = 0.03), Pt(II) (α_s = 0.0075, α_p = 0.013, α_d = 0.025). The relativistic effective core potential (ECP) approximation obtained by Basch and Topiol[50] was used to replace core electrons for Pd and Pt. The effective core potential including relativistic contributions are used to represent 28 and 46 innermost (up to 3d and 4d) electrons of the Pd and Pt atoms (lanl2dz) and standard 6-31+G** basis sets are used. The triple-zeta GTO basis sets[21] for chloride (3s, 3p) and bromide (4s, 4p) were augmented with single 4d and 5d polarization functions for Cl and Br, respectively.

To examine the accuracy of the procedure, the geometrical structure of these complexes has been also optimized with the density functional scheme by the use of the density functional DGauss program.[51] The following Gaussian-type basis sets[51,52] were used: (63321/531/41) for transition metals (Ni, Pd, Pt) and bromine with the uncontracted auxiliary basis sets of (10/5/5); (6321/521/1) for chlorine with the uncontracted auxiliary basis sets of (9/4/4). The geometrical optimizations were self-consistently performed within the local spin density (LSD) approximation. After that, nonlocal corrections proposed by Becke[52] and Perdew[53] for the exchange and correlation interactions have been applied, which can improve the energies of LSD approximation to the similar level as the MP2 method. In addition, the atomic charges of natural bond orbital (NBO) of the equilibrium $[MX_4]^{2-}$ complexes were also analyzed to be investigated the charge transfer of the ligand exchanges.

The potential energy curves of $[MX_4]^{2-}$ dissociating into ($[MX_3]^- + X^-$) have been calculated as a function of the M-Cl distances ranging from 2.258 to 6.00 Å for $[NiCl_4]^{2-}$, from 2.362 to 6.00 Å for $[PdCl_4]^{2-}$, and from 2.388 to 6.00 Å for $[PtCl_4]^{2-}$. For the dissociation reactions, the bond distance variations of *trans* and *cis* M-X bonds are drawn using the results of the DFT calculations. The atomic charge variations of natural bond orbital for the dissociation reactions were also analyzed.

Results and Discussion

Optimized internuclear (M-X) distances of the equilibrium geometrical structures of $[MX_4]^{2-}$ are listed in Table 1. The optimized distances are in good agreement with the previous theoretical[1-23] and experimental[24-44] values. The geometrical structures of $[MX_4]^{2-}$ calculated at the HF, MP2, SDCI, and DFT levels are optimized to four coordinate tetrahedral structure for $[NiX_4]^{2-}$ and square planar structure for $[PdX_4]^{2-}$ and $[PtX_4]^{2-}$. The geometrical structures of the Ni(II), Pd(II), and Pt(II) complexes are characterized by the high or low spin d^8 configuration of the valence electrons.[1-5] That is, the structures of $[MX_4]^{2-}$ are depended on the ordering of the occupied *d*-orbitals. The (M-X) distances of each complex calculated at the HF and MP2 levels are longer than those of the corresponding complexes at the DFT level. The (M-X) distances calculated at the SDCI level are similar to those at the DFT level. The optimized distances of $R_{Ni\text{-}Cl}$ (≅ 2.258 Å), $R_{Pd\text{-}Cl}$ (≅ 2.351 Å), and $R_{Pt\text{-}Cl}$ (≅ 2.367 Å) at the DFT level are smaller than those of $R_{Ni\text{-}Br}$ (≅ 2.332 Å), $R_{Pd\text{-}Br}$ (≅ 2.476 Å), and $R_{Pt\text{-}Br}$ (≅ 2.493 Å), respectively. The optimized $R_{Pt\text{-}Br}$ distance of $[PtBr_4]^{2-}$ is longer than any others, while $R_{Ni\text{-}Cl}$ of $[NiCl_4]^{2-}$ is shorter than any others.

In the experimental analysis[24-38] of the crystal structures, the distances of the Ni-Cl bond of $[NiCl_4]^{2-}$, the Pd-Cl bond of $[PdCl_4]^{2-}$, the Pd-Br bond of $[PdBr_4]^{2-}$, the Pt-Cl bond of $[PtCl_4]^{2-}$, and the Pt-Br bond of $[PtBr_4]^{2-}$ are 2.260, 2.313, 2.444, 2.316, and 2.352 Å, respectively.[24-25] Due to the increases of atomic sizes from Ni to Pt and from Cl to Br, the $R_{Pt\text{-}X}$ distances are longer than $R_{Ni\text{-}X}$ and $R_{Pd\text{-}X}$, and the $R_{M\text{-}Br}$ distances of $[MBr_4]^{2-}$ are longer than $R_{M\text{-}Cl}$ of $[MCl_4]^{2-}$.

Table 1. Optimized (M-X) distances (Å) of the equilibrium geometrical structures of $[MX_4]^{2-}$

	R_{Ni-Cl}	R_{Ni-Br}	R_{Pd-Cl}	R_{Pd-Br}	R_{Pt-Cl}	R_{Pt-Br}
HF	2.329	2.398	2.383	2.501	2.402	2.516
MP2	2.328	2.386	2.366	2.490	2.386	2.504
SDCI	2.256	2.337	2.354	2.475	2.373	2.491
DFT	2.258	2.332	2.351	2.476	2.367	2.493
CNDO[a]	2.275(D_{4h})		2.070		2.311(2.189)	
CNDO[b]	2.183(D_{4h})					
EHT[c]			2.30		2.30	
SCF[d]			2.30			
SCF[e]				2.32		
MP2			2.326[f]		2.329[g]	
MP2			2.39(2.43)[h]		2.364[g]	
LDA			2.31(2.34)[h]			
LDA[i]			2.154(2.192)			
ADF[j]	2.21(2.22)		2.34(2.36)		2.37(2.43)	
ADF[k]			2.360	2.482		
DFT[l]	2.26(T_d)					
DFT	2.38(T_d)[m]		2.329(2.307)[n]	2.364[o]		
DFT	2.32(D_{4h})[m]					
DFT[p]	2.267[p]		2.350[p]			
DFT[p]	2.335[p]		2.402[p]			
exptl	2.26(T_d)[q]		2.307[r]	2.444[s]	2.310[t]	2.445[q]
	2.257[u]		2.313[m]	2.444[m]	2.316[m]	2.352[m]
			2.292[v]		2.309[v]	2.352[w]
			2.309[x]		2.314[y]	
			2.315[z]		2.315[z]	
			2.30[A]		2.305(2.32)[B]	
			2.313[C]	2.444[C]	2.308[C]	2.445[C]
			2.302[D]		3.22[E]	
					2.308[F]	

[a]Ref. 4. [b]Ref. 3. [c]Ref. 23. [d]Ref. 1. [e]Ref. 2. [f]Ref. 17. [g]Ref. 16. [h]Ref. 14. [i]Ref. 5. [j]Ref. 9. [k]Ref. 10. [l]Ref. 6. [m]Ref. 25. [n]Ref. 18. [o]Ref. 19. [p]Ref. 13. [q]Ref. 24. [r]Ref. 26. [s]Ref. 30. [t]Ref. 31. [u]Cited from Ref. 13. [v]Ref. 33. [w]Ref. 29. [x]Ref. 34. [y]Ref. 37. [z]Ref. 35 and 36. [A]Ref. 27. [B]Ref. 32. [C]Ref. 44. [D]Ref. 38. [E]Ref. 39. [F]Ref. 28.

Although the geometries of these complexes have been optimized at the SDCI and DFT levels, all (M-X) distances optimized here are slightly longer than those of the experimental analysis of the crystal structures.[24-38] That is, our calculated (M-X) distances overestimate the experimental ones by 0.02-0.05 Å. The distance difference between the calculated and experimental values is known to be attributed to the crystal environments such as hydrogen bonding and crystal packing. No corresponding crystal compound of the tetrahedral $[NiBr_4]^{2-}$ complexes is known experimentally and not listed in the Table 1.

Using the density functional theory, geometrical optimizations of transition metal(II) tetrahalo complexes ($[MX_4]^{2-}$) were performed by Waizumi *et al*.,[6,7] Deeth group,[12-14] and Burda group.[15-17,20] The geometrical structure of $[NiCl_4]^{2-}$ with tetrahedral geometry is optimized by Waizumi *et al.* and Deeth group. At the DFT level, the R_{Ni-Cl} distances optimized by the two groups are 2.26 and 2.267 Å, respectively. In the results of Deeth group,[13] the calculated (Pd-Cl) distances of $[PdCl_4]^{2-}$ with square planar geometry are a little different (2.35 *vs* 2.313 Å for Pd-Cl) from the corresponding experimental values. In the results of Burda group, R_{Pd-Cl} of $[PdCl_4]^{2-}$ and R_{Pt-Cl} of $[PtCl_4]^{2-}$ at the DFT level are 2.326 and 2.329 Å, respectively. R_{Ni-Cl} (2.21 Å for Ni-Cl), R_{Pd-Cl} (2.34 Å for Pd-Cl), and R_{Pt-Cl} (2.37 Å for Pt-Cl) were also optimized by Liao and Zhang[9] and R_{Pd-Cl} (2.360 Å for Pd-Cl) and R_{Pd-Br} (2.482 Å for Pd-Br) were optimized by Harvey and Reber.[10] The above M-X distances of $[MX_4]^{2-}$ also overestimate from the corresponding experimental values. An overestimation of (M-X) distance increases with increasing the polarity of the (M-X) bond at $[NiCl_4]^{2-}$, $[PdCl_4]^{2-}$, $[PdBr_4]^{2-}$, $[PtCl_4]^{2-}$, and $[PtBr_4]^{2-}$. The interaction between M^{2+} and X^- is a kind of ionic coordinative character, so that the interaction between two ions becomes stronger and the distance between two ions becomes shorter. By replacing Cl^- with Br^-, the van der Waals radius (1.12 Å) of Br^- is longer than the radius (0.97 Å) of Cl^- and the electronegativity of Br^- is weaker than that of Cl^-. Therefore the distances of the M-Br bonds are longer than those of the M-Cl bonds. And these correspond to the difference of the van der Waals radius and the electronegativity between Cl^- and Br^-.

Geometrical structures of axially coordinated tetraaqua and tetrachloro Pt(II) complexes $\{[PtCl_4]^{2-}\cdot(H_2O)_2$,

$[Pt(H_2O)_4]^{2+}\cdot(H_2O)_8\}$ in aqueous solutions have been optimized by the group of Muñoz-Páez.[19] The optimized Pt-Cl distance of equatorial $[PtCl_4]^{2-}$ units in $([PtCl_4]^{2-}\cdot(H_2O)_2$ was found to be 2.352 Å, while the Pt-O distance between metal-water interaction bonded to axial orientation is 3.288 Å. The distance of Pt-Cl is larger than that of Pt-O by about 1 Å. And the value is larger than that (2.77 Å) obtained by Caminiti.[35,36] Although two axially oriented water ligands in $[PtCl_4]^{2-}\cdot(H_2O)_2$ was optimized, an oxygen atom in the water molecule does not bond to planar d^8 center of the Pt(II) complex. Two hydrogen atoms of the water ligand of axially up and down sides hydrogen-bonds to two chloride atoms of *x*- and *y*- axes, respectively. In the $[Pt(H_2O)_4]^{2+}\cdot(H_2O)_8$ complex, eight oxygen atoms of eight water ligands in the second solvation shell only hydrogen-bonds to eight hydrogen atoms of four water molecules inner solvation shell.

To find the minimum of the potential energies of the various geometrical structures of $[MX_4]^{2-}$, the harmonic vibrational frequencies are analyzed at the MP2 and DFT levels and listed in Table 2. Our frequencies are in good agreement with other theoretical[14,18] or experimental[39-46] values. The structure of an isolated $[MX_4]^{2-}$ ion belongs to the D_{4h} symmetry except for $[NiX_4]^{2-}$. The internal vibrational modes of the square planar ion complexes are divided with three Raman modes of a totally symmetric stretching (A_{1g}, ν_1), an antisymmetric stretching (B_{1g}, ν_3), and a bending mode (B_{2g}, ν_4); three IR active modes of a degenerated stretching (E_u, ν_6), an in-plane bending (E_u, ν_7), and out-of-plane bending (A_{2u}, ν_2); and an inactive mode of out-of-plane bending (B_{2u}, ν_5).

In Raman modes of $[MX_4]^{2-}$, our stretching frequencies of A_{1g} and B_{1g} are larger than those of the experimental value by 20 cm^{-1}. While, our bending frequencies of B_{2g} are smaller than those of the experiments. In infrared modes of $[MX_4]^{2-}$, our calculated stretching frequencies of E_u (ν_6) are also larger than those of the experimental results. Furthermore, our three bending frequencies of E_u (ν_7), A_{2u}, and B_{2u} are smaller than those of the experiments. Our calculated frequencies are in accordance with the results of valence force field calculations investigated by Chen *et al.*[44] and Omrani *et al.*[45] The single crystal Raman and infrared spectra of $[MX_4]^{2-}$ should be lower than those of our calculated results. The Raman ν_1 (Pt-Br) stretching frequencies at 237 cm^{-1} and the infrared ν_6 (Pt-Br) degenerated stretching at 264 cm^{-1} are overestimated, while the infrared ν_7 (Br-Pt-Br) in-plane bending frequencies at 111 cm^{-1} is underestimated. The differences between our calculated and experimental frequencies are believed to be from the difference between the calculated structure of gas phase and the experimental structure of a single crystal.

The dissociation energies for the dissociation reactions of $[MX_4]^{2-}$ into ($[MX_3]^- + X^-$) are listed in Table 3. The dissociation energies determined at the DFT level are 4.73 eV for $[NiCl_4]^{2-}$, 4.89 eV for $[NiBr_4]^{2-}$, 4.93 eV for $[PdCl_4]^{2-}$, 5.57 eV for $[PdBr_4]^{2-}$, 5.44 eV for $[PtCl_4]^{2-}$, and 5.87 eV for $[PtBr_4]^{2-}$. The dissociation energies of M-Cl of $[MCl_4]^{2-}$ are smaller than the corresponding energies of M-Br of $[MBr_4]^{2-}$.

Table 2. Vibrational frequency (cm^{-1}) analysis of $[MX_4]^{2-}$ at the DFT level

Modes	$A_{1g}(\nu_1)$	$B_{1g}(\nu_3)$	$B_{2g}(\nu_4)$	$E_u(\nu_6)$	$E_u(\nu_7)$	$A_{2u}(\nu_2)$	$B_{2u}(\nu_5)$
$NiCl_4]^{2-}$							
DFT	267	218	191	289	142	157	78
$NiBr_4]^{2-}$							
DFT	182	146	140	237	114	124	66
$PdCl_4]^{2-}$							
DFT	322	281	194	351	172	189	120
MM [a]	327	266	190	364	159	206	101
DFT [a]	310	284	173	336	180	175	102
DFT [b]	295	264	143	316	149	144	19
DFT [c]	308	274	199	334	163	190	123
exptl [c]	307	274	198	332	170	189	
exptl [d]	305	275	195				
exptl [e]				336	193		110
exptl [f]	303	275	164				
exptl [g]	307	275	198	334	178	187	123
exptl [h]	306	271	195	334	190	170	
$[PdBr_4]^{2-}$							
DFT	213	176	125	278	133	139	71
DFT [c]	190	170	129	259	112	137	68
exptl [c]	190	171	127	258	126	137	
exptl [d]	188	178	127				
exptl [e]				260	140	130	85
exptl [f]	188	172	102				
exptl [g]	190	170	129	261	143	136	68
$[PtCl_4]^{2-}$							
DFT	341	311	199	339	174	190	149
DFT [c]	329	305	198	322	160	193	144
exptl [c]	329	304	196	321	176	194	
exptl [d]	330	303	195				
exptl [f]	330	312	171				
exptl [i]	325		190		170		
exptl [j]	329	304	195				
$[PtBr_4]^{2-}$							
DFT	237	195	128	264	111	137	86
DFT [c]	205	189	129	242	118	140	85
exptl [c]	205	188	128	232	131	139	
exptl [d]	205	190	125				
exptl [f]	208	194	106				

[a]Ref. 18. [b]Ref. 14. [c]Ref. 44. [d]Ref. 43. [e]Ref. 40. [f]Ref. 42. [g]Ref. 45. [h]Ref. 46. [i]Ref. 39. [j]Ref. 41.

Our energy of Pd-Cl in $[PdCl_4]^{2-}$ is larger than the previous calculated energies,[14] while the energy of $[NiCl_4]^{2-}$ is smaller than the theoretical and experimental values.[6,7,9,15,23] On the basis of the EHT method, the geometrical structures of the transition metal complexes of chlorides and its molecular species were optimized by Ponec and Řeřicha.[23] The dissociation energies of the M-Cl bonds in $[PdCl_4]^{2-}$ and $[PtCl_4]^{2-}$ are only obtained from the potential energy difference between $[MCl_4]^{2-}$ and it asymptotes. The dissociation energies (0.24 eV for $[PdCl_4]^{2-}$, 0.58 eV for $[PtCl_4]^{2-}$) calculated with the EHT method are too smaller than our calculated values at the DTF level. The binding energies of

Table 3. Dissociation energies[a] (eV) for the dissociation reactions of $[MX_4]^{2-}$ into $([MX_3]^- + X^-)$

	E_{Ni-Cl}	E_{Ni-Br}	E_{Pd-Cl}	E_{Pd-Br}	E_{Pt-Cl}	E_{Pt-Br}
HF	4.11	4.42	4.29	5.09	5.05	5.62
MP2	4.39	4.53	4.82	5.33	5.26	5.74
SDCI	4.66	4.86	4.84	5.42	5.31	5.82
DFT	4.73	4.89	4.93	5.57	5.44	5.87
EHT[b]			0.24		0.58	
LDA[c]			3.73			
			3.26			
DFT[d]	6.27					
exptl[e]	5.50					
	5.82					

[a]Ref. 14. and 7. "The dissociation energies of Ni-Xe, Pd-Xe. and Pt-Xe are 0, 0.37, and 0.60 eV, respectively. The dissociation energies of $[CuCl_4]^{2-}$ and $[CuBr_4]^{2-}$ are 6.25 and 6.4 eV, respectively." [b]Ref. 23. [c]Ref. 15. [d]Ref. 6. [e]Cited from Ref. 9.

the metal-olefin π-complexes of $[M(Cl_3)(C_2H_4)]^-$ are obtained by Noell and Hay.[21-22] The metal-olefin π-complexes are formed by the interaction between the anion of $[PtCl_3]^-$ and π-orbital of C_2H_4. The binding energies of $[Pd(Cl_3)(C_2H_4)]^-$ and $[Pt(Cl_3)(C_2H_4)]^-$ are 0.54 and 1.24 eV, respectively. By the studies of Waizumi *et al.*,[6,7] the dissociation energy of $[CuCl_4]^{2-}$ and $[CuBr_4]^{2-}$ are 6.25 and 6.40 eV, respectively. These values are larger than those of the other complexes. In the results of Burda *et al.*,[15] the dissociation energies of diatomic molecules of NiXe, PdXe, and PtXe are 0.00, 0.37, and 0.60 eV, respectively.

Under C_{2v} symmetry constraint, potential energy curves for the dissociation energies of $[MX_4]^{2-}$ dissociating into $([MX_3]^- + X^-)$ at the DFT level is drawn in Figure 1. The potential energies of the equilibrium geometrical structures of $[MX_4]^{2-}$ are set equal to zero, respectively. All energies are adiabatic value and are in units of eV. The ground potential energy curves of $[MX_4]^{2-}$ are interconnected with the attractive states from the $([MX_3]^- + X^-)$ asymptotes. Under the symmetry constraint, the intersystem crossings or internal conversions for the dissociation reactions of $[MX_4]^{2-}$ into $([MX_3]^- + X^-)$ can not take place on the potential curves. The ground tetrahedral structure for $[NiX_4]^{2-}$ and the ground square planar structures for $[PdX_4]^{2-}$ and $[PtX_4]^{2-}$ have T_d and D_{4h} symmetries, respectively. In $[MX_4]^{2-}$, the transition Ni(II), Pd(II), and Pt(II) metals have five n*d*, one (n+1)*s*, and three (n+1)*p* atomic valence orbitals which form bonding combinations to the surrounding ligands or remain nonbonding. The electronic configuration of the ground $^3F_4$ state for Ni(II), Pd(II), and Pt(II) is $[core]ns^2np^6nd^8$. In square planar $[MX_4]^{2-}$ complexes, the ground electronic state of $[PdX_4]^{2-}$ and $[PtX_4]^{2-}$ is $^1A_1$ state. For the transition Pd and Pt metal, $2a_{1g}$ orbital emerging from d_{z2} orbital and $2b_{1g}$ orbital from d_{x2-y2} orbital are HOMO and LUMO, respectively. In the valence orbital of metal, the b_{2g} orbital emerging from d_{xy} orbigtal, e_g orbital from d_{xz} and d_{yz} orbitals, and a_{2u} orbital from p_z orbital are nonbonding orbital. The $3a_{1g}$ orbital emerging from 4s orbital and e_u orbital from p_x and p_y orbitals are bonding orbital. The stable square planar $[MX_4]^{2-}$ complexes have 13 valence orbitals and possess a total of 16 valence electrons. In the tetrahedral $[NiX_4]^{2-}$ complexes, a t_3 orbital of Ni(II) emerges from $3d_{x2-y2}$ ($2b_{1g}$ in square planer), $3d_{xz}$ (e_g), and $3d_{yz}$ (e_g) orbitals and a e orbital from $3d_{z2}$ ($2a_{1g}$ in square planar) and $3d_{xy}$ (b_{2g}) orbitals. Eight valence electrons of metals fill in e and t_3 orbitals. The t_3 orbital is HOMO. In t_3 orbital, the four electrons have a high spin (triplet state) configuration as a stable species. The t_3 orbital has Ni–X antibonding character. The ground electronic state of $[NiX_4]^{2-}$ is $^3T_2$ state.

By removing one ligand from the transition metal $[MX_4]^{2-}$ complexes, the geometry of the $[MX_3]^-$ fragment is formed a T-shaped structure with C_{2v}-symmetry. In the reaction path, all of the orbitals are basically unperturbed when one ligand is removed except for $2a_{1g}$ (d_{z2}) and $2b_{1g}$ (d_{x2-y2}) orbitals. The

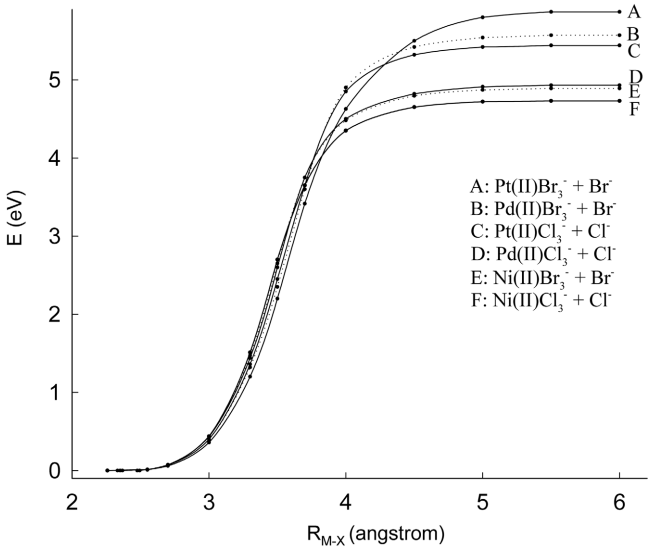

Figure 1. Potential energy curves for the dissociation reactions of $[MX_4]^{2-}$ into $([MX_3]^- + X^-)$ keeping C_{2v} symmetry. All energies are adiabatic values and are in units of eV.

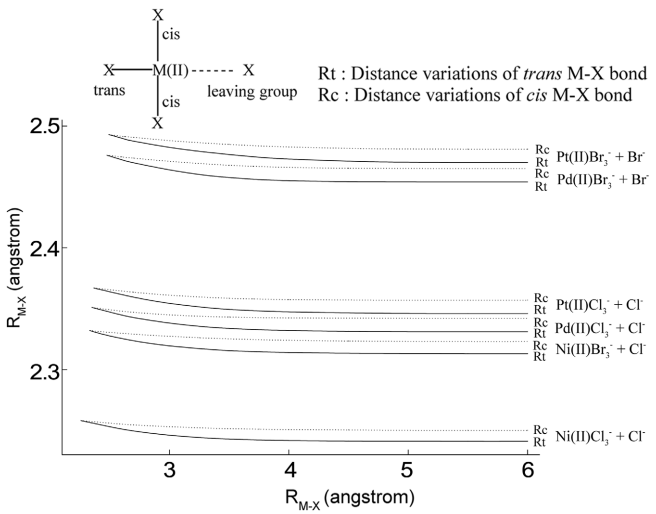

Figure 2. *trans* and *cis* (M-X) distance variation curves for the dissociations of $[MX_4]^{2-}$ into $([MX_3]^- + X^-)$. Solid line : Rt. Dot line : Rc.

$2a_{1g}$ (d_{z2}) and $2b_{1g}$ (d_{x2-y2}) orbitals are HOMO and LUMO and are slightly stabilized. The rest of the orbitals (b_{2g}, e_g, and a_{2u}) in $[MX_4]^{2-}$ remain energetically unchanged to the b_1, a_2, $1b_2$, and $2b_2$ orbitals in $[MX_3]^-$. The ground electronic state of $[MX_3]^-$ is $^1A_1$ state. The configurations for the ground $^1S_0$ state of Cl^- and Br^- are [core]$3s^23p^6$ and [core]$4s^24p^6$, respectively. The ligands (Cl^-, Br^-) are a σ donor type which is pointed toward the metal and there are two electrons in it.

For the dissociation reactions of ($[MX_3]^- \cdots X^-$), the energy gap of the potential curve of $[PtBr_4]^{2-}$ is larger than those of the potential curves for the other dissociation reactions. The energy differences for the potential energy curves of $[MBr_4]^{2-}$ are larger than those for the potential energy curves of $[MCl_4]^{2-}$. The dissociation energy of $[NiCl_4]^{2-}$ is smaller than those of the dissociation reactions of $[PdCl_4]^{2-}$ and $[PtCl_4]^{2-}$. The interaction between M^{2+} and X^- becomes stronger and the distance between two ions becomes shorter. By the coordination bonds emerging from the cation-anion pair of [M^{2+} + $4X^-$], the dissociation energies and the relative energy gaps of $[MX_4]^{2-}$ dissociating into ($[MX_3]^-$ + X^-) are found to be relatively large. By replacing $[NiCl_4]^{2-}$ with $[PtBr_4]^{2-}$, the van der Waals radius (≅1.30 Å for Pt, ≅1.12 Å for Br) of $[PtBr_4]^{2-}$ is longer than those (≅1.15 Å for Ni, ≅1.28 Å for Pd, ≅0.97 Å for Cl) of the other complexes. That is, the distance of the Pt-Br bond is longer than those of Ni-Cl and Pd-Br. And the bond breaking of $[PtBr_4]^{2-}$ dissociating into ($[PtBr_3]^-$ + Br^-) takes place longer than those of the other complexes.

Distance variations of *trans* and *cis* (M-X) bonds for dissociation of $[MX_4]^{2-}$ into ($[MX_3]^-$ + X^-) are represented in Figure 2, which are the results of the DFT calculation. The distance variations of the opposite (M-X) bond (*trans*-position) and the neighboring (M-X) bond (*cis*-position) for the dissociation reactions are denoted as **Rt** and **Rc**, respectively. The differences of the **Rt** variations for the dissociation reactions are 0.017 Å for $[NiCl_4]^{2-}$, 0.019 Å for $[NiBr_4]^{2-}$, 0.020 Å for $[PdCl_4]^{2-}$, 0.022 Å for $[PdBr_4]^{2-}$, 0.021 Å for $[PtCl_4]^{2-}$, and 0.023 Å for $[PtBr_4]^{2-}$ and the differences of **Rc** are 0.008 Å for $[NiCl_4]^{2-}$, 0.009 Å for $[NiBr_4]^{2-}$, 0.009 Å for $[PdCl_4]^{2-}$, 0.011 Å for $[PdBr_4]^{2-}$, 0.010 Å for $[PtCl_4]^{2-}$, and 0.012 Å for $[PtBr_4]^{2-}$. The slopes of the *trans* and *cis* Pt-Br distance variations for the dissociation of $[PtBr_4]^{2-}$ into ($[PtBr_3]^-$ + Br^-) are steeper than those of the other *trans* and *cis* M-X distance variations, that is, the distance variations (**Rt**, **Rc**) of *trans* and *cis* Pt-Br bonds of $[PtBr_4]^{2-}$ are larger than any other **Rt** and **Rc**. The differences between **Rt** and **Rc** are 0.009 Å for $[NiCl_4]^{2-}$, 0.010 Å for $[NiBr_4]^{2-}$, 0.011 Å for $[PdCl_4]^{2-}$, 0.011 Å for $[PdBr_4]^{2-}$, 0.011 Å for $[PtCl_4]^{2-}$, and 0.011 Å for $[PtBr_4]^{2-}$. The difference between **Rt** and **Rc** for $[PtBr_4]^{2-}$ dissociating into ($[PtBr_3]^-$ + Br^-) is wider than those of the other dissociation reactions.

At each (M-X) distance, the *trans* (M-X) distance is shorter than those of two *cis* (M-X) bonds. That is, the distance variations (**Rt**) of the (M-X) bond at the *trans* position are larger than those (**Rc**) of two *cis* (M-X) bonds. The variations of $\mathbf{Rt}_{(M\text{-}Br)}$ and $\mathbf{Rc}_{(M\text{-}Br)}$ are larger than those of $\mathbf{Rt}_{(M\text{-}Cl)}$ and $\mathbf{Rc}_{(M\text{-}Cl)}$, respectively. With the increasing of atomic sizes from Ni to Pt and from Cl to Br, the van der Waals radius of $[PtBr_4]^{2-}$ is longer than those of the other complexes. That is, the Pt-Br bond has a relatively long range interaction of ($[PtBr_3]^- \cdots Br^-$). The Ni-X bond rupture in $[NiX_4]^{2-}$ take place at shorter than $R_{(Ni\text{-}X)}$ ≅3.0-4.0 Å, while the Pt-X bond rupture takes place near $R_{Pt\text{-}X}$ ≅3.5-4.5 Å. As the internuclear distance of M-X increase, the leaving X^- group is dissociated to be negative anion state. The electronic charge density of the *trans* M-X bond is moved to central M(II). Therefore the distance of the *trans* M-X bond is shorter than those of two *cis* M-X bonds.

Atomic charges of the equilibrium geometrical structures of $[MX_4]^{2-}$ and two internuclear distances of ($[MX_3]^- \cdots X^-$) are listed in Table 4. Our charge values are in good agreement with the previous calculated results.[9,16,17] At the equilibrium geometries, the charge value of M(II) is positive, whereas those of four X atoms are negative. Depending on M(II), the atomic charges of M(II) and four X atoms are different from each other. The charge density of Ni(II) is larger than those of Pd(II) and Pt(II). That is, the charge of Ni(II) is more positive than those of Pd(II) and Pt(II). The negative charge value of Cl in $[NiCl_4]^{2-}$ is larger than those of Cl in $[PdCl_4]^{2-}$ and $[PtCl_4]^{2-}$ and the negative charge value of Br in $[NiBr_4]^{2-}$ is also larger than those of Br in $[PdBr_4]^{2-}$ and $[PtBr_4]^{2-}$. The atomic charges of Cl and Br in $[NiX_4]^{2-}$ are more negative than those of corresponding $[PdX_4]^{2-}$ and $[PtX_4]^{2-}$, respectively. Using the density functional theory (DFT), the atomic charges of the equilibrium geometrical structures of $[MX_4]^{2-}$ were investigated by Liao and Zhang[9] and Burda group,[16,17] In the study of Liao and Zhang, Q_{Ni} and Q_{Cl} for $[NiCl_4]^{2-}$ are 0.133 and −0.53 au, respectively. The charges are so smaller than ours. Meanwhile the other charges for $[PdCl_4]^{2-}$ and for $[PtCl_4]^{2-}$ are similar to ours.

As the ($M \cdots X$) distance of ($[MX_3]^- \cdots X^-$) increases, the atomic charge variations of the *trans* X atom and leaving X^- group are relatively large, while the charge variations of M(II) and two *cis* X atoms are small. From the equilibrium geometry of $[MX_4]^{2-}$ to its asymptotes, the atomic charge of *trans* X atom changes to more positive value, while the atomic charge of leaving X^- group changes to more negative value. That is, the average charge variations between $[NiCl_4]^{2-}$ and ($[NiCl_3]^-$ + Cl^-) are 0.037 au for *trans* X atom and −0.153 au for leaving X^- group and the average charge variations between $[PtBr_4]^{2-}$ and ($[PtBr_3]^-$ + Br^-) are 0.237 au for *trans* X atom and −0.360 au for leaving X^- group. The charge variation of *trans* Br atom of $[MX_4]^{2-}$ is more positive than these of *trans* Cl atom of $[MX_4]^{2-}$, while the variation of leaving Br^- group is more negative than these of leaving Cl^- group. The charge variation of Pt(II) is more positive than those of Ni(II) and Pd(II).

In asymptote of ($[MX_3]^-$ + X^-), the leaving X^- group dissociates to become a negative anion state. The atomic charge of the leaving halogen atom varies from X^0 to X^-. Therefore, the atomic charge of the central M(II) moves to

Table 4. Natural bond orbital (NBO) charges (au) of the equilibrium geometrical structures ($[MX_4]^{2-}$) and two internuclear distances ($[MX_3]^-\cdots X^-$) (Å)

		equilibrium			Theo. Value		R_{MX} = 3.5	R_{MX} = 6.0
		HF	MP2	DFT	MP2	MP[q]	DFT	DFT
$NiCl_4]^{2-}$	Q_{Ni}[a]	0.915	0.848	0.714		0.133	0.721	0.733
	Q_{Cl}[b,m]	−0.904	−0.830	−0.821		−0.53	−0.807	−0.784
	Q_{Cl}[n]	−0.904	−0.830	−0.821		−0.932	−0.974	
$NiBr_4]^{2-}$	Q_{Ni}[c]	0.910	0.830	0.693			0.706	0.718
	Q_{Br}[d,m]	−0.867	−0.782	−0.773			−0.722	−0.693
	Q_{Cl}[n]	−0.867	−0.782	−0.773			−0.905	−0.966
$PdCl_4]^{2-}$	Q_{Pd}[e]	0.852	0.780	0.656	0.537[o]	0.62	0.660	0.678
	Q_{Cl}[f,m]	−0.788	−0.695	−0.689	−0.631[o]	−0.66	−0.618	−0.574
	Q_{Cl}[n]	−0.788	−0.695	−0.689			−0.838	−0.903
$[PdBr_4]^-$	Q_{Pd}[g]	0.865	0.555	0.512			0.543	0.551
	Q_{Br}[h,m]	−0.716	−0.639	−0.633			−0.535	−0.475
	Q_{Cl}[n]	−0.716	−0.639	−0.633			−0.815	−0.920
$[PtCl_4]^{2-}$	Q_{Pt}[i]	0.892	0.527	0.519	0.57[p] 0.37[p]	0.48	0.566	0.577
	Q_{Cl}[j,m]	−0.723	−0.632	−0.625	−0.64[p] −0.40[p]	−0.62	−0.551	−0.505
	Q_{Cl}[n]	−0.723	−0.632	−0.625			−0.798	−0.888
$[PtBr_4]^{2-}$	Q_{Ptk}	0.592	0.423	0.403			0.491	0.503
	Q_{Br}[l,m]	−0.648	−0.581	−0.576			−0.462	−0.339
	Q_{Cl}[n]	−0.648	−0.581	−0.576			−0.812	−0.936

[a]Atomic charges of Ni(II) in $[NiCl_4]^{2-}$. [b]Atomic charges of Cl in $[NiCl_4]^{2-}$. [c]Atomic charges of Ni(II) in $[NiBr_4]^{2-}$. [d]Atomic charges of Br in $[NiBr_4]^{2-}$. [e]Atomic charges of Pd(II) in $[PdCl_4]^{2-}$. [f]Atomic charges of Cl in $[PdCl_4]^{2-}$. [g]Atomic charges of Pd(II) in $[PdBr_4]^{2-}$. [h]Atomic charges of Br in $[PdBr_4]^{2-}$. [i]Atomic charges of Pt(II) in $[PtCl_4]^{2-}$. [j]Atomic charges of Cl in $[PtCl_4]^{2-}$. [k]Atomic charges of Pt(II) in $[PtBr_4]^{2-}$. [l]Atomic charges of Br in $[PtBr_4]^{2-}$. [m]*trans*-X atom of $[MX_4]^{2-}$ dissociating into ($[MX_3]^-\cdots X^-$). [n]*leaving* X group of $[MX_4]^{2-}$ dissociating into ($[MX_3]^-\cdots X^-$). [o]Ref. 17. [p]Ref. 16. [q]Ref. 9.

the leaving X^- group and the atomic charge of M(II) become more positive state. To reduce the positive charge value of M(II) in ($[MX_3]^-\cdots X^-$), the atomic charge moves from *trans* X atom to the central M(II). Along the M-X bond rupture coordinate, the moving direction of the atomic charge from the *trans* M-X bond to the leaving X^- group is the same as the direction of the M-X bond dissociation of ($[MX_3]^-\cdots X^-$). By the movement of the atomic charge, the interaction between M(II) and *trans* X atom occurs strongly. Simultaneously, the bond distance between M(II) and *trans* X atom becomes shorter. If the charge transfer from *trans* X atom to leaving X^- group does not occur, the bond distance between M(II) and *trans* X atom may be nearly constant. It can be confirmed that there is strong interaction between M(II) and *trans* X atom. For the M-X bond dissociation, the atomic charge variations of M(II) and *trans* X atom are in line with the distance variations of *trans* X atom and leaving X^- group.

Conclusions

We optimized the equilibrium geometrical structures of ($[MX_4]^{2-}$: M=Pd(II), Pt(II); X=Cl^-, Br^-) with square planar geometry and ($[NiX_4]^{2-}$: X=Cl^-, Br^-) with tetrahedral geometry. Our optimized (M-X) distances of the equilibrium $[MX_4]^{2-}$ structures are in good agreement with the previous theoretical and experimental analysis. The dissociation energies of $[MX_4]^{2-}$ dissociating into ($[MX_3]^- + X^-$) determined at the DFT level are found to be 4.73-5.87 eV. The dissociation energy of M-Br in $[MBr_4]^{2-}$ is larger than the corresponding energy of M-Cl in $[MCl_4]^{2-}$. Our dissociation energy of M-X is similar to the theoretical and experimental values. In the potential energy curve, the bond dissociations ranging from 2.5 to 5.0 Å were occurred. The bond breakings of ($[NiCl_3]^-\cdots Cl^-$) and ($[PtBr_3]^-\cdots Br^-$) occur at the shortest and longest distances, respectively. The energy gap of ($[PtBr_3]^-\cdots Br^-$) is larger than those of the other dissociation reactions. The interaction between M^{2+} and X^- becomes stronger and the relative distance between two ions becomes shorter. The dissociation energy of $[MX_4]^{2-}$ dissociating into ($[MX_3]^- + X^-$) are found to be relatively large.

As internuclear M-X distance of ($[MX_3]^-\cdots X^-$) increases, the distances of three M-X bonds of $[MX_3]^-$ decrease. The distance variations (Rt) of the *trans* (M-X) bond are larger than those (Rc) of two *cis* (M-X) bonds. The slopes of Rt and Rc for the dissociation of $[NiCl_4]^{2-}$ into ($[NiCl_3]^- + Cl^-$) are flatter than those of the other Rt and Rc. The variations of $Rt_{(M-Br)}$ and $Rc_{(M-Br)}$ are larger than those of the corre-

sponding $Rt_{(M-Cl)}$ and $Rc_{(M-Cl)}$, respectively. The variation difference between $Rt_{(Pt-Br)}$ and $Rc_{(Pt-Br)}$ is wider than those of the other variations. As the internuclear distance of M-X increase, the leaving X^- group is dissociated to be a negative anion state. The charge densities of the *trans* and *cis* M-X bonds are moved to a central M(II). Therefore the distances of the *trans* and *cis* M-X bonds is shorter than those of the equilibrium $[MX_4]^{2-}$ structure. Along the (M-X) bond rupture coordinate, the charge variations of M(II) and *trans* X atom are more positive, while the charge variations of the leaving X^- group are more negative. To reduce the positive charge characters of M(II) in $[MX_3]^-$, the charge transfer from *trans* X atom to leaving X^- group occurs and the bond distances between M(II) and *trans* X atom becomes shorter. It can be confirmed that the charge density variations of M(II) and *trans* X atom are in line with the distance variations of *trans* X atom and the leaving X^- group. The charge transfer from *trans* X atom to leaving X^- group greatly contributes to the distance variations of *trans* (M-X) bonds and the bond dissociation of the leaving X^- group in the solvation system.

Acknowledgment. We thank the Korea Research Foundation (KRF) for supporting this work through the Basic Science Research Institute program (KRF-2002-015-CP0161). The support from Gyeongsang National University Research Fund is also acknowledged.

References

1. Tondello, E.; Di Sipio, L.; De Michelis, G.; Oleari, L. *Inorg. Chim. Acta* **1971**, *5*, 305.
2. Messmer, R. P.; Interrante, L. V.; Johnson, K. H. *J. Am. Chem. Soc.* **1974**, *96*, 3847.
3. Pelikán, P.; Liška, M. *Coll. Czech. Chem. Commun.* **1982**, *47*, 1556.
4. Boèa, R. *Int. J. Quant. Chem.* **1987**, *31*, 941.
5. Bickelhaupt, M.; Ziegler, T.; Schleyer, P. von R. *Organomet.* **1995**, *14*, 2288.
6. Waizumi, K.; Masuda, H.; Einaga, H.; Fukushima, N. *Bull. Chem. Soc. Jpn.* **1993**, *66*, 3648.
7. Kang, D. M.; Kim, S. G.; Lee, S. J.; Park, J. K.; Park, K. M.; Shin, S. C. *Bull. Korean Chem. Soc.* **2005**, *26*, 1390.
8. Gilardoni, F.; Weber, J.; Bellafrouh, K.; Daul, C.; Güdel, H.-U. *J. Chem. Phys.* **1996**, *104*, 7624.
9. Liao, M.-S.; Zhang, Q.-er. *Inorg. Chem.* **1997**, *36*, 396.
10. Harvey, P. D.; Reber, C. *Can. J. Chem.* **1999**, *77*, 16.
11. Park, J. K.; Cho, Y. G.; Lee, S. S.; Kim, B. G. *Bull. Korean Chem. Soc.* **2004**, *20*, 85.
12. Deeth, R. J.; Elding, L. I. *Inorg. Chem.* **1996**, *35*, 5019.
13. Bray, M. R.; Deeth, R. J.; Paget, V. J.; Sheen, P. D. *Int. J. Quant. Chem.* **1996**, *61*, 85.
14. Deeth, R. J. *Chem. Phys. Lett.* **1996**, *261*, 45.
15. Burda, J. V.; Runeberg, N.; Pyykkö, P. *Chem. Phys. Lett.* **1998**, *288*, 635.
16. Burda, J. V.; Zeizinger, M.; Šponer, J.; Leszczynski, J. *J. Chem. Phys.* **2000**, *113*, 2224.
17. Zeizinger, M.; Burda, J. V.; Šponer, J.; Kapsa, V.; Leszczynski, J. *J. Phys. Chem. A* **2001**, *105*, 8086.
18. Lienke, A.; Klatt, G.; Robinson, D. J.; Koch, K. R.; Naidoo, K. J. *Inorg. Chem.* **2001**, *40*, 2352.
19. Ayala, R.; Marcos, E. S.; Daz-Moreno, S.; Solë, V. A.; Muòoz-Pãez, A. *J. Phys. Chem. B* **2001**, *105*, 7588.
20. Burda, J. V.; Zeizinger, M.; Leszczynski, J. *J. Chem. Phys.* **2004**, *120*, 1253.
21. Hay, P. J. *J. Am. Chem. Soc.* **1981**, *103*, 1390.
22. Noell, J. O.; Hay, P. J. *Inorg. Chem.* **1982**, *21*, 14.
23. Ponec, R.; Řeřicha, R. *J. Organomet. Chem.* **1988**, *431*, 549.
24. Albanese, A.; Staley, D. L.; Rheingold, A. L.; Burmeister, J. L. *Acta Cryst.* **1989**, *C45*, 1128.
25. Bridgeman, A. J.; Gerloch, M. *Mol. Phys.* **1993**, *79*, 1195.
26. Allen, F. H.; Kennard, O. *Chem. Des. Autom. News* 8, **1993**, *1*, 31.
27. Bell, J. P.; Hall, D.; Waters, T. N. *Acta Cryst.* **1960**, *21*, 440.
28. Mais, R. H. B.; Owston, P. G.; Wood, A. M. *Acta Cryst.* **1972**, *B28*, 393.
29. Kroening, R. F.; Rush, R. M.; Martin Jr., D. S.; Clardy, J. C. *Inorg. Chem.* **1974**, *13*, 1366.
30. Martin Jr., D. S.; Bonte, J. L.; Rush, R. M.; Jacobson, R. A. *Acta Cryst.* **1975**, *B31*, 2538.
31. Ohba, S.; Sato, S.; Saito, Y. *Acta Cryst.* **1983**, *B39*, 49.
32. Ohba, S.; Saito, Y. *Acta Cryst.* **1984**, *C40*, 1639.
33. Templeton, D. H.; Templeton, L. K. *Acta Crystallogr.* **1985**, *A41*, 365.
34. Takazawa, H.; Ohba, S.; Saito, Y. *Acta Cryst.* **1988**, *B44*, 580.
35. Caminiti, R.; Sadun, C.; Basanisi, M.; Carbone, M. *J. Mol. Liquid* **1996**, *70*, 55.
36. Caminiti, R.; Carbone, M.; Sadun, C. *J. Mol. Liquid* **1998**, *75*, 149.
37. Bengtsson, L. A.; Oskarsson, A. *Acta Chem. Scand.* **1992**, *46*, 707.
38. Valle, G.; Ettorre, R. *Acta Crystallogr.* **1994**, *C50*, 1221.
39. Hiraishi, J.; Shimanouchi, T. *Spectrochim. Acta* **1966**, *22*, 1483.
40. Perry, C. J.; Athans, D. P.; Young, E. F.; Durig, J. R.; Mitchell, B. R. *Spectrochim. Acta Part* **1967**, *A23*, 1137.
41. Hiraishi, J.; Nakagawa, I.; Shimanouchi, T. *Spectrochim. Acta Part* **1968**, *A24*, 819.
42. Goggin, P. L.; Mink, J. *J. Chem. Soc. Dalton Trans.* **1974**, 1479.
43. Degen, I. A.; Rowlands, A. J. *Spectrochim. Acta Part* **1991**, *A47*, 1263.
44. Chen, Y.; Christensen, D. H.; Nielsen, O. F.; Hyldtoft, J.; Jacobsen, C. J. H. *Spectrochim. Acta* **1995**, *A51*, 595.
45. Omrani, H.; Cavagnat, R.; Sourisseau, C. *Spectrochim. Acta* **2000**, *A56*, 1645.
46. Parker, S. F.; Herman, H.; Zimmerman, A.; Williams, K. P. *J. Chem. Phys.* **2000**, *261*, 261.
47. Frish, M. J.; Trucks, G. W.; Head-Gordon, M. H.; Gill, P. M. W.; Wong, M. W.; Foresman, J. B.; Johnson, B. G.; Schlegel, H. B.; Robb, M. A.; Replogle, E. S.; Gomperts, R.; Andres, J. L.; Raghavachari, K.; Binkley, J. S.; Gonzalez, C.; Martin, R. L.; Fox, D. J.; Defrees, D. J.; Baker, J.; Stewart, J. J. P.; Pople, J. A. *Gaussian 03*; Gaussina Inc.: Pittsburgh, PA, 2003.
48. Dolg, M.; Wedig, U.; Stoll, H.; Preuss, H. *J. Chem. Phys.* **1987**, *86*, 866.
49. Andrae, D.; Hausserman, U.; Dolg, M.; Stoll, U. H.; Preuss, H. *Theo. Chim. Acta* **1990**, *77*, 123.
50. Basch, H.; Topiol, S. *J. Chem. Phys.* **1979**, *71*, 802.
51. Andzelm, J.; Wimmer, E. *J. Chem. Phys.* **1992**, *96*, 1280; Andzelm, J.; Wimmer, E.; Salahub, D. R.; The Challenge of d- and f-Electrons: Theory and Computation; Salahub, D. R.; Zerner, M. C., Eds.; *ACS Symposium Series*, No. 394; American Chemical Society: Washington D. C. 1989; p 228 and references therein; Andzelm, J. *Density Functional Methods in Chemistry*; Labanowski, J.; Andzelm, J., Eds.; Springer-Verlag: New York, 1991; p 155 and references therein.
52. Becke, A. D. *The Challenge of d- and f-Electrons: Theory and Computation*; Salahub, D. R.; Zerner, M. C. *ACS Symposium Series*, No. 394; American Chemical Society: Washington, D.C. 1989; p 166; Becke, A. D. *Phys. Rev.* **1988**, *A38*, 3098.
53. Perdew, J. P. *Phys. Rev.* **1986**, *B33*, 8822.